Dynamic Data-Driven Estimation of Power System Linear Sensitivity Distribution Factors

Yu Christine Chen, Alejandro D. Domínguez-García, and Peter W. Sauer

Abstract This chapter presents a method to compute power system linear sensitivity distribution factors in near real-time without relying on an offline system power flow model. Instead, the data-driven estimation of power sensitivities (DEPS) methods use high-frequency synchronized data collected from phasor measurement units to estimate injection shift factors (ISFs), from which other distribution factors can be computed. Distribution factors are commonly used in power system security analysis applications that rely on an offline database of line parameters and breaker status. These databases are updated only periodically and may not reflect the actual system. Being rooted in the paradigm of Dynamic Data Driven Applications Systems (DDDAS), the DEPS methods are adaptive to undetected changes in the system operating point and topology, and so it is favorable over a traditional model-based counterpart. Furthermore, the work presented here shows how the adaptability of the DEPS methods to system changes can be improved by exploiting a sparse representation of the vector of desired ISFs and casting the estimation problem into a sparse vector recovery problem. The accuracy and scalability of the DEPS methods are demonstrated through numerical case studies involving large-scale test systems.

The work described in this chapter was made possible by the funding provided by the US Department of Energy for "The Future Grid to Enable Sustainable Energy Systems," an initiative of the Power Systems Engineering Research Center, by the Consortium for Electric Reliability Technology Solutions, and by the Natural Sciences and Engineering Research Council of Canada under its Postgraduate Scholarship Program.

Y. C. Chen (✉)
The University of British Columbia, Vancouver, BC, Canada
e-mail: chen@ece.ubc.ca

A. D. Domínguez-García · P. W. Sauer
University of Illinois at Urbana-Champaign, Urbana, IL, USA
e-mail: aledan@illinois.edu; psauer@illinois.edu

© The Author(s), under exclusive license to Springer Nature Switzerland AG 2026

E. P. Blasch et al. (eds.), *Handbook of Dynamic Data Driven Applications Systems*,
https://doi.org/10.1007/978-3-031-88574-7_14

Keywords Compressive sensing · Distribution factors · Least-squares errors estimation · Phasor measurement units · Power system monitoring · Sensitivity · Synchrophasors

1 Introduction

In order to monitor and maintain operational reliability, power system operators perform several static security analysis computations. For example, the results of real-time contingency analysis help operators determine whether or not the system would meet operational reliability requirements in case of an outage in any single particular asset (e.g., a generator or a transmission line), a condition known as *N-1 security*, and further whether or not corrective actions (e.g., generation re-dispatch in a constrained system) are required [1, 2]. These studies may include repeated computations (for each credible contingency) of power flow solutions using the full nonlinear power flow model or a linearized power flow model. To reduce the computational burden of evaluating repeated power flow solutions, linear sensitivity distribution factors, such as injection shift factors (ISFs), power transfer distribution factors (PTDFs), line outage distribution factors (LODFs), and outage transfer distribution factors (OTDFs), are used to predict the effect of an operating point change [3].

Traditional model-based studies are not ideal since the results depend on an accurate model with the up-to-date network topology, which may not be available due to erroneous telemetry from remotely monitored circuit breakers. Such deficiencies in network situational awareness, including knowledge of transmission line statuses, have contributed to the cause of numerous major North American blackouts [1, 2]. For example, in the 2011 San Diego blackout, operators could not detect that certain lines were overloaded or close to being overloaded because the network model was not up-to-date [1]. Furthermore, the results from model-based studies may not be applicable if the actual system evolution does not match any predicted operating points due to unforeseen circumstances such as equipment failure, large variations in generation or load, or unpredictable levels of renewable generation. Thus, traditional model-based techniques in general no longer satisfy the needs of monitoring and protection tasks, and therefore, it is important to develop power system monitoring tools that are adaptive to changes in operating point and topology, in particular, to estimate distribution factors without relying on a system model. With respect to the need for real-time network analytics, phasor measurement units (PMUs) are an enabling technology for the development of such data-driven monitoring tools, and in particular on methods that apply the Dynamic Data Driven Applications Systems (DDDAS) paradigm [4]. Unlike traditional system measurements, PMUs measure voltages and currents at a very high speed (usually 30 measurements per second) [5], and phasors measured at different locations by different devices are time-synchronized with Global Positioning System clocks [6].

This chapter presents methods to estimate linear sensitivity distribution factors while exploiting measurements obtained from PMUs in near real-time without the use of a power flow model. Based in the DDDAS paradigm, the methods are dubbed as *data-driven estimation of power sensitivities* (DEPS), and they were originally proposed in [7–10]. Linear sensitivity distribution factors are widely known and used in power system analyses [3, 11]. Existing approaches to computing distribution factors typically employ so-called DC approximations, which can provide fast contingency screening [12]. They do not, however, have the flexibility of adapting to real-time changes in network topology or generation and load variations, which can significantly affect the actual linear sensitivities. Recent attention has been given to the computation of the LODF due to their role in revealing cascading outages [13, 14]. The LODF-based approaches still depend on an accurate model of the system.

Unlike traditional model-based approaches, the DEPS methods presented here rely on measurements of active-power bus injections and line flows obtained from PMUs and small fluctuations inherent to load and generation to compute the linear sensitivities through linear least-squares errors (LSE) estimation. While the LSE-based approach is shown to accurately compute ISFs (a type of distribution factors from which others can be calculated) with undetected system topology changes, the LSE formulation necessitates at least as many sets of synchronized measurements as unknown ISFs [8]. For a large power system, such a restriction may be ill-advised in, e.g., real-time contingency analysis, since power systems are constantly undergoing changes and operators often need to quickly determine whether or not the current system is secure. To address the accuracy and scalability issue, a more computationally efficient method is presented here, which exploits a sparse representation (i.e., one in which many elements are zero) of the ISFs, to estimate them using fewer sets of measurements than unknown ISFs.

2 Preliminaries

Power system distribution factors are linearized sensitivities used in, e.g., online contingency analysis, generation re-dispatch, and congestion relief [3]. A key distribution factor is the ISF, which quantifies the redistribution of the power flowing in each transmission line following a change in generation or load on a particular bus with a slack bus constraint included. The ISF captures the sensitivity of the flow through a line with respect to changes in generation or load. Other distribution factors include the PTDF, the LODF, and the OTDF [12], all of which can easily be derived from the ISF.

2.1 Definition of Injection Shift Factor

Let $\mathcal{L}$ denote the set of n_l transmission lines and $\mathcal{B}$ the set of n buses in the system; the ISF of line $L_{k\text{-}\ell} \in \mathcal{L}$ (assume positive real power flow from bus k to ℓ measured at bus k) with respect to bus $i \in \mathcal{B}$, which is denoted here by $\Psi^i_{k\text{-}\ell}$, as the linear approximation of the sensitivity of the active-power flow in line $L_{k\text{-}\ell}$ with respect to the active-power injection at bus i with the location of the slack bus specified and all other quantities constant. Suppose P_i varies by a small amount ΔP_i and denote by $\Delta P^i_{k\text{-}\ell}$ the change in active-power flow in line $L_{k\text{-}\ell}$ (measured at bus k) resulting from ΔP_i. Then it follows that

$$\Psi^i_{k\text{-}\ell} := \frac{\partial P_{k\text{-}\ell}}{\partial P_i} \approx \frac{\Delta P^i_{k\text{-}\ell}}{\Delta P_i}. \tag{1}$$

Traditionally, ISFs, along with other distribution factors, have been computed offline based on a model of the power system including its topology and pertinent parameters, which is established via a historic database of parameter values and equipment status. However, a major source of error in power system security analyses results from the equipment database failing to reflect the up-to-date state of the power grid. The DEPS methods avoid this error by using online measurements to estimate the real-time status of the grid, bypassing the need for an offline model altogether. Before delving into the details of the DEPS methods, the model-based approach to compute ISFs is described first so as to motivate the need for a DDDAS-based framework.

2.2 Traditional Model-Based Approach to ISF Computation

The industry-standard approach for security analyses is to represent the power system via a nonlinear mathematical model that implicitly relies on offline information of the system including its topology (i.e., line parameters and breaker status) and operating point (i.e., voltages and currents). The nonlinear model commonly used in power system security analyses comprises the so-called power flow equations. As already mentioned, the information needed to construct the power flow equations may not be up-to-date with real-time system operations, which may then lead to unexpected errors in power system security computations. Nevertheless, traditionally, ISFs are computed from a perturbation analysis of the power flow equations by linearizing them around a particular operating point.

Let V_i and θ_i, respectively, denote the voltage magnitude and angle at bus i; additionally, let P_i and Q_i, respectively, denote the active and reactive-power injection (generator or load) at bus i. Then, the static behavior of a power system can be described by the power flow equations, which can be written compactly as

$$g(x, P, Q) = 0, \tag{2}$$

where $x = [\theta_1, \ldots, \theta_n, V_1, \ldots, V_n]^T$, $P = [P_1, \ldots, P_n]^T$, $Q = [Q_1, \ldots, Q_n]^T$, and $g : \mathbb{R}^{2n} \times \mathbb{R}^n \times \mathbb{R}^n \to \mathbb{R}^{2n}$. In (2), the dependence on network parameters, such as line series and shunt impedances, is implicitly considered in the function $g(\cdot)$.

Suppose a solution for (2) is obtained at (x_0, P_0, Q_0), i.e., $g(x_0, P_0, Q_0) = 0$, and assume $g(\cdot)$ is continuously differentiable with respect to x and P at (x_0, P_0, Q_0). Let $x = x_0 + \Delta x$ and $P = P_0 + \Delta P$. Then, assume that ΔP and Δx are sufficiently small, which can approximate $g(x, P, Q_0)$ as

$$g(x, P, Q_0) \approx g(x_0, P_0, Q_0) + J\Delta x + D\Delta P, \tag{3}$$

where

$$J = \frac{\partial g}{\partial x}\Big|_{(x_0, P_0, Q_0)} \text{ and } D = \frac{\partial g}{\partial P}\Big|_{(x_0, P_0, Q_0)}.$$

Since $g(x_0, P_0, Q_0) = 0$, and assuming that Δx and ΔP are small, then $g(x, P, Q_0) \approx 0$ and it follows from (3) that

$$0 \approx J\Delta x + D\Delta P. \tag{4}$$

Further, since J is the Jacobian of the power flow equations, which is assumed to be invertible around (x_0, P_0, Q_0), (4) can be rearranged to obtain

$$\Delta x \approx -J^{-1} D\Delta P. \tag{5}$$

Next, consider the active-power flow through line $L_{k\text{-}\ell}$ as $P_{k\text{-}\ell} = h_{k\text{-}\ell}(x)$, where $h_{k\text{-}\ell} : \mathbb{R}^{2n} \to \mathbb{R}$. Under the same small Δx assumption, one can obtain an expression for small variations $\Delta P_{k\text{-}\ell}$ due to Δx as follows:

$$\Delta P_{k\text{-}\ell} = c\Delta x, \tag{6}$$

where $c = \frac{\partial h_{k\text{-}\ell}}{\partial x}\Big|_{x_0}$. Substituting (5) into (6), it follows that

$$\Delta P_{k\text{-}\ell} \approx -cJ^{-1} D\Delta P. \tag{7}$$

The derivation of the sensitivity vector $-cJ^{-1}D$ relies on the linearization of the nonlinear power flow equations around an operating point, and therefore, it depends on the system topology and operating point.

For certain power system applications (such as congestion relief), the so-called DC assumptions are further used to simplify the linear sensitivities derived in (2)–(7) (see, e.g., [3]). Let $\widetilde{B} = \text{diag}\{b_{k\text{-}\ell}\}$, which is a diagonal matrix whose entries are $b_{k\text{-}\ell}$, denoting the susceptance of line $L_{k\text{-}\ell}$, for each $L_{k\text{-}\ell} \in \mathcal{L}$. Also, denote the line-to-bus incidence matrix by $A = [\ldots, a_{k\text{-}\ell}, \ldots]^T$, where $a_{k\text{-}\ell} \in \mathbb{R}^n$ is a

vector in which the k^{th} entry is 1 and the ℓ^{th} entry is -1. Then, by using the DC approximations [(i) the system is lossless, (ii) $V_i = 1$ p.u. for all $i \in \mathcal{B}$, and (iii) $\theta_i - \theta_j << 1$ for all $i, j \in \mathcal{B}$ [3]], the expression in (6) simplifies to

$$\Delta P_{k\text{-}\ell} \approx \widetilde{B}_{k\text{-}\ell} A B^{-1} \Delta P, \tag{8}$$

where $\widetilde{B}_{k\text{-}\ell}$ is the row in $\widetilde{B}$ that corresponds to line $L_{k\text{-}\ell}$, and $B = A^T \widetilde{B} A$. Then, by defining $\Psi_{k\text{-}\ell} = [\Psi^1_{k\text{-}\ell}, \ldots, \Psi^i_{k\text{-}\ell}, \ldots, \Psi^n_{k\text{-}\ell}]^T$, the model-based linear sensitivity factors for line $L_{k\text{-}\ell}$ with respect to active-power injections at all buses are given by

$$\Psi_{k\text{-}\ell} = \widetilde{B}_{k\text{-}\ell} A B^{-1}. \tag{9}$$

Under the DC assumptions, not only are the resulting distribution factors inflexible against variations in system topology, but they also remain constant through possible operating point variations under a single topology, e.g., generation and load fluctuations.

2.3 Problem Statement

The traditional model-based approach to ISF computation outlined in (2)–(9) is not ideal since accurate and up-to-date network topology, parameters, and operating point are required. Moreover, under the so-called DC assumptions, the model-based ISFs do not vary with system operating changes. Hence, the aims are to (i) eradicate the reliance on power flow models for computing distribution factors and (ii) improve adaptability of computed distribution factors to changes occurring in the system. With regard to adaptability, a method is presented here to estimate distribution factors using only PMU measurements obtained in near real-time without relying on a power flow model of the system.

Role of DEPS Methods in Power System Security Analyses Prior to formalizing the DEPS methods to estimate ISFs, a high-level discussion is warranted on how such methods and other DDDAS-based tools are envisioned to fit within the existing suite of traditional model-based security analysis applications. Placing the discussion within the flowchart in Fig. 1, traditional model-based security assessment and monitoring tools (shaded in orange) include, e.g., real-time contingency analysis, generation re-dispatch in the case that the previous assessment flags a violation, and state estimation to compute all system states (including voltages and transmission line flows). As mentioned previously, mismatches between the model and the actual system can cause significant errors in the results of these analyses. There are conceivably two ways to address the issues that arise due to the mismatches: (i) to develop power system online monitoring tools without relying on a model of the system and (ii) to develop efficient and robust tools to detect and identify topology

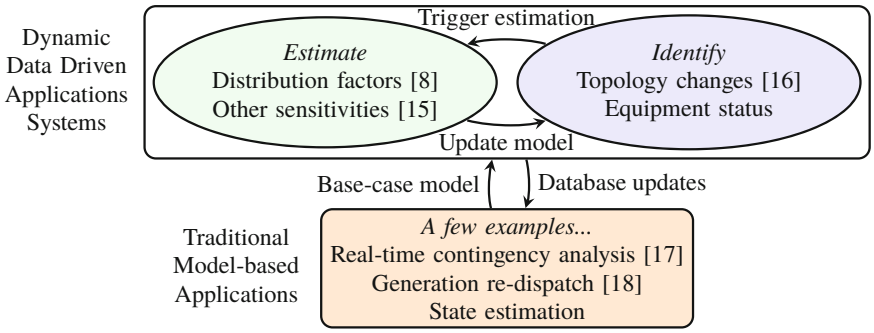

Fig. 1 Placing DEPS methods (shaded in green) within the context of other DDDAS-based tools (shaded in blue) and traditional model-based power system security analyses (shaded in orange)

changes, so as to update the offline model in a timely fashion (see, e.g., [16, 19][1]). The DEPS methods presented in this chapter fall squarely into the first category, shaded in green in Fig. 1. Although the focus here is the estimation of ISFs, the DEPS methods can be extended to estimate other linear sensitivities, such as entries in the power flow Jacobian matrix [15, 20]. Collectively, the DDDAS-based methods can provide real-time updates to the equipment database used in model-based applications, or they may improve the performance of specific applications (see, e.g., [17, 18]). In return, a base-case model constructed from a historical database used in the model-based analyses can be useful for the DDDAS-based tools to, e.g., provide a warm start for estimation algorithms.

3 Dynamic Data-Driven ISF Computation

This section presents the formulation of the DDDAS-based method to compute the ISFs without relying on a power flow model. To this end, let $P_i(t)$ denote the active-power injection at bus i at time t; similarly, for $\Delta t > 0$ is sufficiently small, let $P_i(t + \Delta t)$ denote the active-power injection at time $t + \Delta t$. Define $\Delta P_i(t) = P_i(t + \Delta t) - P_i(t)$; then, based on the definition of the ISF in (1), it ensures that

$$\Psi^i_{k\text{-}\ell} \approx \frac{\Delta P^i_{k\text{-}\ell}(t)}{P_i(t + \Delta t) - P_i(t)}. \tag{10}$$

In order to obtain $\Psi^i_{k\text{-}\ell}$, the $\Delta P^i_{k\text{-}\ell}(t)$'s are also needed, but they are not readily available from PMU measurements. On the other hand, it is assumed that the net

[1] The work presented in [16, 19] was supported under the DDDAS-based 2014 AFOSR-NSF Program.

variation in active-power flow through line $L_{k\text{-}\ell}$, denoted by $\Delta P_{k\text{-}\ell}(t)$, is available. This net variation is expressed as the sum of active-power variations in line $L_{k\text{-}\ell}$ due to active-power injection variations at each bus i:

$$\Delta P_{k\text{-}\ell}(t) = \Delta P^1_{k\text{-}\ell}(t) + \cdots + \Delta P^n_{k\text{-}\ell}(t). \tag{11}$$

By substituting (10) into (11), (11) can be rewritten as

$$\Delta P_{k\text{-}\ell}(t) \approx \Delta P_1(t)\Psi^1_{k\text{-}\ell} + \cdots + \Delta P_n(t)\Psi^n_{k\text{-}\ell},$$

where $\Psi^i_{k\text{-}\ell} \approx \frac{\Delta P^i_{k\text{-}\ell}}{\Delta P_i}$, $i = 1, \ldots, n$. Suppose $m + 1$ sets of synchronized measurements are available. Let $\Delta P_i[j] = P_i((j+1)\Delta t) - P_i(j\Delta t)$, and $\Delta P_{k\text{-}\ell}[j] = P_{k\text{-}\ell}((j+1)\Delta t) - P_{k\text{-}\ell}(j\Delta t)$, $j = 1, \ldots, m$; and define $\Delta P_{k\text{-}\ell} = [\Delta P_{k\text{-}\ell}[1], \ldots, \Delta P_{k\text{-}\ell}[j], \ldots, \Delta P_{k\text{-}\ell}[m]]^T$, $\Delta P_i = [\Delta P_i[1], \ldots, \Delta P_i[j], \ldots, \Delta P_i[m]]^T$. Let $\Psi_{k\text{-}\ell} = [\Psi^1_{k\text{-}\ell}, \ldots, \Psi^i_{k\text{-}\ell}, \ldots, \Psi^n_{k\text{-}\ell}]^T$; then, it follows that

$$\Delta P_{k\text{-}\ell} \approx \left[\Delta P_1 \cdots \Delta P_i \cdots \Delta P_n\right] \Psi_{k\text{-}\ell}. \tag{12}$$

For ease of notation, let ΔP represent the $m \times n$ matrix $[\Delta P_1, \ldots, \Delta P_i, \ldots, \Delta P_n]$; then, the system in (12) can be compactly written as

$$\Delta P_{k\text{-}\ell} \approx \Delta P \Psi_{k\text{-}\ell}. \tag{13}$$

Equation (13) hypothesized that the relationship between $\Delta P_{k\text{-}\ell}$ and $\Psi_{k\text{-}\ell}$ is approximately linear. Let $e \in \mathbb{R}^m$ denote the combination of inherent deterministic error arising from the linearization assumption and stochastic error arising from measurement noise. As is customary, the measurement error process is assumed to be additive white Gaussian noise with zero mean and variance σ^2 [21]. By explicitly representing these errors in the formulation, (13) becomes

$$\Delta P_{k\text{-}\ell} = \Delta P \Psi_{k\text{-}\ell} + e. \tag{14}$$

Then, the task is to estimate the vector $\Psi_{k\text{-}\ell}$ using, e.g., linear least-squares errors (LSE) estimation.

3.1 LSE-Based Algorithms for ISF Computation

Assuming $m \geq n$, then (14) is an overdetermined system of equations, from which one can obtain the least-squares estimate of the ISF vector for line $L_{k\text{-}\ell}$, $\Psi_{k\text{-}\ell} = [\Psi^1_{k\text{-}\ell}, \ldots, \Psi^i_{k\text{-}\ell}, \ldots, \Psi^n_{k\text{-}\ell}]^T$, by solving the following LSE estimation problem:

$$\min_{\Psi_{k\text{-}\ell}} e^T e. \tag{15}$$

The solution to this problem is given by (see, e.g., [22])

$$\widehat{\Psi}_{k\text{-}\ell} = (\Delta P^T \Delta P)^{-1} \Delta P^T \Delta P_{k\text{-}\ell}. \tag{16}$$

Next, the ideas presented above are demonstrated for an overdetermined system in (14) via an example.

Example 1 (3-Machine 9-Bus System) This example illustrates the concepts described above with the Western Electricity Coordinating Council (WECC) 3-machine 9-bus system. In order to simulate PMU measurements of slight fluctuations in active-power injection at each bus, time-series data is created for the active-power injection at each bus. In particular, the injection at bus i, denoted by P_i, is given by

$$P_i[j] = P_i^0[j] + \sigma_1 P_i^0[j] v_1 + \sigma_2 v_2, \tag{17}$$

where $P_i^0[j]$ is the nominal power injection at bus i at instant $j\Delta t$, and v_1 and v_2 are pseudorandom values drawn from standard normal distributions with zero mean and standard deviations $\sigma_1 = 0.1$ and $\sigma_2 = 0.1$, respectively. The first component of variation, $\sigma_1 P_i^0[j] v_1$, represents the inherent fluctuations in generation and load, while the second component, $\sigma_2 v_2$, represents random measurement noise.

In the WECC example, 601 sets of synchronized line flow and bus injection data are acquired, i.e., $m = 600$. For each set of bus injection data obtained at a particular time instant, we compute the power flow, allowing the slack bus to absorb all power imbalances, and compute the active-power flow through line $L_{k\text{-}\ell}$ for that time instant. By taking the difference between consecutive line flow measurements, the vector $\Delta P_{k\text{-}\ell}$ in (14) is obtained. Similarly, the regressor matrix ΔP in (14) is obtained by taking the differences between consecutive values of bus power injections. Suppose a 0.5 per-unit (p.u.) increase is applied to G_2 at bus 2 and the slack bus absorbs the resulting power imbalance. Table 1 shows a comparison between the corresponding effect on three lines computed from (i) the actual power flow solution, (ii) a linearized DC model-based approximation, and (iii) the DEPS method discussed here. It is evident that the DEPS method provides more accurate results than the model-based one.

Table 1 Comparison of ISFs obtained for Example 1

Line	Actual (p.u.)	Model-based (p.u.)	LSE (p.u.)
$\Delta P_{4\text{-}5}$	−0.2970	−0.3196	−0.3022
$\Delta P_{4\text{-}6}$	−0.1734	−0.1804	−0.1749
$\Delta P_{7\text{-}8}$	+0.1838	+0.1804	+0.1830

Two key assumptions are made in (16): (i) the ISFs are approximately constant over $m + 1$ measurements, and (ii) matrix ΔP has full column rank. The first restriction can be relaxed by employing weighted least-squares estimation [8]. Further, by implementing the standard or weighted LSE estimation recursively, we avoid the lag time required to acquire a sufficiently large set of PMU data. This work was first proposed in [7] and expanded in [8], where advantages of the LSE-based ISF estimation approach over the traditional model-based one are illustrated in the context of contingency analysis and generation re-dispatch with IEEE test systems. Next, a sparse method to estimate ISFs with fewer sets of measurements than unknowns is presented.

3.2 A Sparse Representation Approach

As discussed in Sect. 3.1, if $m \geq n$, then (14) is an overdetermined system and can be solved for $\Psi_{k\text{-}\ell}$ via LSE estimation as in (16). However, for a large system with many buses, it may not be prudent to require such a large number of measurement sets before an estimate can be computed. Further, the adaptability of the DEPS approach to system changes would be improved if fewer sets of data are required. Thus, this section focuses on solving for $\Psi_{k\text{-}\ell}$ in (14) for $m < n$, i.e., obtaining a solution when (14) is an underdetermined system of equations.

The computation approach presented in this section is inspired by the field of compressive sensing (CS) (see, e.g., [23]), and its applications to image processing, where a typical problem is to compress a large image (i.e., to reduce irrelevant or redundant image data in order to store or transmit the image efficiently), and subsequently reconstruct the image from its compressed representation. Recently, CS ideas have been applied to the identification of multiple line outages in power systems [24]. CS theory asserts that, by exploiting their sparsity, certain classes of signals can be recovered from fewer samples or measurements than those needed in traditional methods such as LSE estimation (see, e.g., [25, 26]). Specifically, the problem of recovering a sparse signal can be cast as one where the objective is to minimize the ℓ_0-norm[2] of the signal to be recovered.

3.2.1 Sparsifying Injection Shift Factors

In the setting considered, the signal of interest, the ISF vector $\Psi_{k\text{-}\ell}$, is not necessarily sparse; therefore, DEPS needs to search for an appropriate linear coordinate transformation M, such that $\Psi_{k\text{-}\ell} = M c_{k\text{-}\ell}$, where $c_{k\text{-}\ell}$ is a sparse vector, i.e., one in which many elements are zero. In order to compute $\Psi_{k\text{-}\ell}$ with $m < n$ measurements,

[2] For a vector with finite support, the ℓ_0-norm is defined as the number of its entries that are nonzero (see, e.g., [23]).

DEPS first needs to reorder its entries by the electrical distance of each bus to the line $L_{k\text{-}\ell}$, a main advantage of which is its independence from the slack bus location. Then, a *difference transformation* (to be defined below) is applied to the sorted signal. This leads to a sparse representation of the ISFs, which allows us to cast the ISF estimation problem into a sparse vector recovery problem. Once this problem is solved, the inverse difference transformation is applied to the resulting sparse vector estimate to finally obtain an estimate of the ISF vector.

Reordering by Electrical Distance Here it is assumed that prior to online estimation, a base-case system model is available that consists of all relevant nominal system topology, parameter, and operating point information. Using this nominal model, a one-time computation of the electrical distance from each bus to line $L_{k\text{-}\ell}$ is performed.

Denote the bus admittance matrix by[3] $\mathbf{Y} = [\mathbf{Y}_{ik}]$. Then, apply Kirchhoff's current law at each bus and express the current injected into each bus i from the ground node as

$$\mathbf{I}_i = \sum_{k=1}^{n} \mathbf{Y}_{ik}\mathbf{V}_k, \tag{18}$$

where $\mathbf{V}_k$, $k = 1, \ldots, n$, is the voltage at bus k. Let $\mathbf{Z} = [\mathbf{Z}_{ki}] = \mathbf{Y}^{-1}$, then the voltage at bus k can be expressed as

$$\mathbf{V}_k = \sum_{i=1}^{n} \mathbf{Z}_{ki}\mathbf{I}_i. \tag{19}$$

On the other hand, the current through the line connected from bus k to ℓ is

$$\mathbf{I}_{k\text{-}\ell} = (\mathbf{V}_k - \mathbf{V}_l)\mathbf{y}_{k\text{-}\ell} + \mathbf{V}_k\mathbf{y}^{\text{sh}}_{k\text{-}\ell}, \tag{20}$$

where $\mathbf{y}_{k\text{-}\ell}$ is the admittance of the line connecting buses k and ℓ, and $\mathbf{y}^{\text{sh}}_{k\text{-}\ell}$ is the shunt admittance at bus k. Substitution of (19) into (20) results in

$$\mathbf{I}_{k\text{-}\ell} = \left(\sum_{i=1}^{n} \mathbf{Z}_{ki}\mathbf{I}_i - \sum_{i=1}^{n} \mathbf{Z}_{li}\mathbf{I}_i\right)\mathbf{y}_{k\text{-}\ell} + \sum_{i=1}^{n} \mathbf{Z}_{ki}\mathbf{I}_i\mathbf{y}^{\text{sh}}_{k\text{-}\ell}, \tag{21}$$

and after rearranging, $\mathbf{I}_{k\text{-}\ell} = \sum_{i=1}^{n} \mathbf{a}^{i}_{k\text{-}\ell}\mathbf{I}_i$ is obtained, where the electrical distance between bus i and line $L_{k\text{-}\ell}$ is given by [27]:

$$\mathbf{a}^{i}_{k\text{-}\ell} = (\mathbf{Z}_{ki} - \mathbf{Z}_{li})\,\mathbf{y}_{k\text{-}\ell} + \mathbf{Z}_{ki}\mathbf{y}^{sh}_{k\text{-}\ell}. \tag{22}$$

[3] Bolded symbols denote complex-valued quantities.

Sorting the vector $\Psi_{k\text{-}\ell}$ according to the electrical distance as defined in (22) yields the rearranged vector $\Psi_{k\text{-}\ell,s}$ as

$$\Psi_{k\text{-}\ell,s} = [\Psi^1_{k\text{-}\ell,s}, \ldots, \Psi^i_{k\text{-}\ell,s}, \ldots, \Psi^n_{k\text{-}\ell,s}]^T,$$

such that index $i \leq j$ if $|\mathbf{a}^i_{k\text{-}\ell}| \geq |\mathbf{a}^j_{k\text{-}\ell}|$. The intuition behind this particular approach is as follows: the injections at buses that are electrically far away from line $L_{k\text{-}\ell}$ often have little effect on the active-power flow through line $L_{k\text{-}\ell}$ as compared to nearer ones. Hence, after reordering of the buses based on electrical distance, the sorted signal, $\Psi_{k\text{-}\ell,s}$, is characterized by smooth segments separated by sporadic jumps. Therefore, the difference between consecutive elements is likely small; as detailed below, this is the premise upon which a linear transformation can be defined that results in a sparse representation of $\Psi_{k\text{-}\ell,s}$.

Applying a Difference Transformation This transformation is defined via the difference between consecutive elements of $\Psi_{k\text{-}\ell,s}$:

$$c^i_{k\text{-}\ell} = \Psi^i_{k\text{-}\ell,s} - \Psi^{i+1}_{k\text{-}\ell,s}, \quad c^n_{k\text{-}\ell} = \Psi^n_{k\text{-}\ell,s}. \tag{23}$$

In matrix form, the difference transformation, defined in (23), can be written as $c_{k\text{-}\ell} = M\Psi_{k\text{-}\ell,s}$, where $M = [m_{ij}]$, with $m_{ij} = 1$ if $j = i$, $m_{ij} = -1$ if $j = i + 1$, and $m_{ij} = 0$, otherwise. If the difference transformation in (23), indeed, results in $c_{k\text{-}\ell}$ being sparse, one can then exploit ideas from CS to compute the estimate $\widehat{c}_{k\text{-}\ell}$ using $m < n$ measurement data sets. To recover $\widehat{\Psi}_{k\text{-}\ell,s}$ (denoting the estimate for $\Psi_{k\text{-}\ell,s}$), the inverse difference transformation is applied as follows:

$$\widehat{\Psi}_{k\text{-}\ell,s} = M^{-1}\widehat{c}_{k\text{-}\ell}. \tag{24}$$

3.2.2 Sparse ISF Vector Recovery

Through sorting and transforming the original ISF vector $\Psi_{k\text{-}\ell}$, it is assumed the post-transformation signal $c_{k\text{-}\ell}$ to be sparse. Since the elements of $\Psi_{k\text{-}\ell}$ have been sorted by electrical distance, one can also rearrange the columns of ΔP accordingly, and denote the reordered matrix as ΔP_s. Using ΔP_s, the original problem of estimating $\Psi_{k\text{-}\ell}$ such that (14) is satisfied is transformed to the problem of estimating $c_{k\text{-}\ell}$ such that $\Delta P_{k\text{-}\ell} = \Phi c_{k\text{-}\ell}$ is satisfied, where $\Phi = \Delta P_s M^{-1}$ is the so-called measurement matrix. Since $c_{k\text{-}\ell}$ is assumed to be a sparse vector, one can cast the ISF vector estimation problem as an optimization program where the objective is to minimize $||c_{k\text{-}\ell}||_0$—the number of nonzero elements in $c_{k\text{-}\ell}$:

$$\begin{aligned} &\min_{c_{k\text{-}\ell}} ||c_{k\text{-}\ell}||_0 \\ &\text{subject to } \Delta P_{k\text{-}\ell} = \Phi c_{k\text{-}\ell}. \end{aligned} \tag{25}$$

The optimization problem in (25) is NP-hard due to the unavoidable combinatorial search [23]. There are numerous classes of computational techniques for solving sparse approximation problems like the one in (25); two major ones are greedy pursuit methods and convex relaxation methods [28]. Greedy pursuit algorithms refine a solution iteratively by choosing one or more components of ΔP_s that yield the greatest improvement until a convergence criterion is met. Convex relaxation algorithms replace the combinatorial problem in (25) with a convex optimization problem by relying on the close approximation of the ℓ_1-norm to the ℓ_0-norm when the vector is sparse.

Utilizing a sparse representation for injection shift factors first proposed by Y. C. Chen et al. [9], the sparsity-exploiting approach provides distribution factor estimates with accuracy comparable to LSE-based approaches, but using fewer sets of synchronized measurements. The example presented next illustrates the effectiveness of the difference transformation in (23) and two sparse vector recovery algorithms on an IEEE test system.

Example 2 (IEEE 14-Bus System) Consider the IEEE 14-bus system (see, e.g., [29]). The model-based linear sensitivity ISF vector of line $L_{2\text{-}3}$, $\Psi_{2\text{-}3}$, is computed using the partial derivative definition in (10) by linearizing the nonlinear AC power flow equations. After reordering by electrical distance, these model-based ISFs are plotted in Fig. 2. While the rearranged signal is fairly smooth except at buses 1, 12, and 13, the vector has only one zero element. In order to get a sparse representation, the difference transformation defined in (23) to the signal shown in Fig. 2 is applied to obtain the signal depicted in Fig. 3 (also recorded in Table 2, column 3), which contains many zero or near-zero elements with the same sharp edges as in Fig. 2.

In this example, in order to recover the sparse vector $c_{2\text{-}3}$, one can use orthogonal matching pursuit (OMP) in the class of greedy pursuit algorithms (see, e.g., [23]) and a log-barrier algorithm in the class of convex relaxation algorithms (see, e.g., [23]). Inspection of Table 2 reveals that the log-barrier algorithm achieves

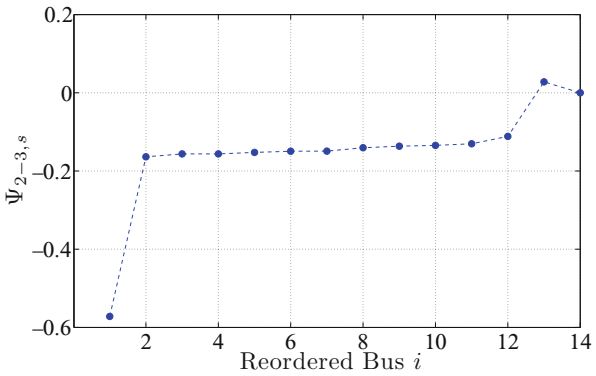

Fig. 2 IEEE 14-bus system: Reordered ISFs of line $L_{2\text{-}3}$ with respect to each bus (not sparse)

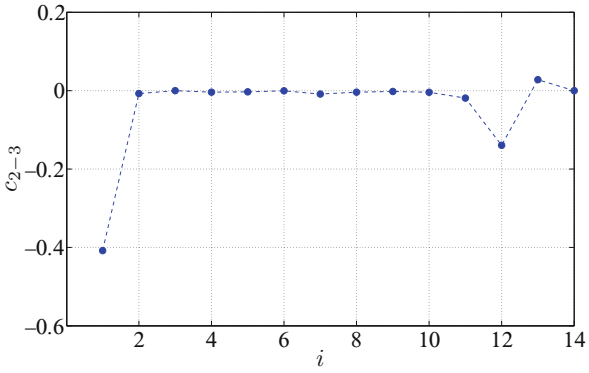

Fig. 3 IEEE 14-bus system: Transformed ISFs of line $L_{2\text{-}3}$ with respect to each bus (sparse)

higher accuracy than OMP, which is verified by comparing the ℓ_2-norm of the error in each estimate as compared to the benchmark model-based $c_{2\text{-}3}$, as shown in the last row of Table 2. Further, the log-barrier algorithm with $m = 10, 13$ leads to more accurate estimates than those obtained using the LSE-based approach with $m = 14$. On the other hand, with OMP, only the estimate obtained with $m = 13$ is superior to the LSE-based approach with $m = 14$. However, the estimate obtained using the LSE-based method with $m = 20$ is more accurate than all of the estimates obtained with $m < n$. Thus, there are some trade-offs between the level of accuracy and the number of measurements required.

4 Case Studies

This section illustrates the application and effectiveness of the DEPS methods presented in Sect. 3 using the IEEE 300-bus test system and the 2383-bus Polish power system. While the DEPS algorithms have not been deployed on real-world power system networks due to proprietary concerns about the data, they have been validated using standard IEEE test systems with highly encouraging results, as described in the remainder of this section. The proof-of-concept numerical case studies presented here are crucial to demonstrate the efficacy of the DEPS algorithms prior to real-world implementation. The simulation tool MATPOWER [30] is used throughout to compute relevant transmission line flow measurements from some synthetic power injection profiles generated using (17).

Table 2 Comparison of $\widehat{c}_{2\text{-}3}$ for the IEEE 14-bus system obtained in Example 2

			$\widehat{c}^i_{2\text{-}3}$ (via OMP)			$\widehat{c}^i_{2\text{-}3}$ (via log-barrier)			$\widehat{c}^i_{2\text{-}3}$ (via LSE)	
i	$\Psi^i_{2\text{-}3}$	$c^i_{2\text{-}3}$	$m = 7$	$m = 10$	$m = 13$	$m = 7$	$m = 10$	$m = 13$	$m = 14$	$m = 20$
1	0	−0.4082	−0.2916	−0.4178	−0.4094	−0.3924	−0.4154	−0.4111	−0.4124	−0.4080
2	0.0279	−0.0074	−0.2286	0	−0.0051	−0.0003	−0.0010	−0.0037	−0.0020	−0.0069
3	−0.5719	0	0.1971	−0.0085	−0.0005	0.0001	−0.0002	−0.0012	−0.0025	0.0001
4	−0.1637	−0.0039	−0.0202	0	−0.0023	−0.0001	−0.0051	−0.0023	−0.0009	−0.0041
5	−0.1115	−0.0030	−0.0040	0.0010	−0.0063	−0.0000	−0.0036	−0.0054	−0.0070	−0.0013
6	−0.1304	−0.0004	0	−0.0049	0.0010	−0.0108	−0.0012	0.0002	0.0002	−0.0011
7	−0.1563	−0.0087	0	−0.0011	−0.0046	−0.0015	−0.0013	−0.0036	0.0002	−0.0118
8	−0.1563	−0.0039	−0.0082	0	−0.0089	−0.0123	−0.0077	−0.0084	−0.0104	−0.0021
9	−0.1524	−0.0021	0	−0.0130	0	0.0000	−0.0001	−0.0011	−0.0018	−0.0011
10	−0.1494	−0.0041	0	0	−0.0030	−0.0003	−0.0032	−0.0027	−0.0022	−0.0050
11	−0.1404	−0.0189	−0.1587	−0.0219	−0.0175	−0.0244	−0.0163	−0.0174	−0.0169	−0.0189
12	−0.1345	−0.1394	0	−0.1414	−0.1408	−0.1328	−0.1416	−0.1409	−0.1417	−0.1393
13	−0.1366	0.0279	0	0.0315	0.0270	0.0290	0.0252	0.0269	0.0273	0.0279
14	−0.1491	0	0	0.0002	−0.0010	−0.0072	−0.0016	−0.0011	−0.0017	0.0003
$\|\|\widehat{c}_{2\text{-}3} - c_{2\text{-}3}\|\|_2$			0.3761	0.0225	0.0087	0.0265	0.0138	0.0094	0.0147	0.0043

4.1 IEEE 300-Bus System

In the case study involving the IEEE 300-bus test system [31], the focus is on the ISFs of lines $L_{272\text{-}268}$, $L_{30\text{-}73}$, and $L_{112\text{-}148}$ with respect to each bus in the system. These lines are selected because they are typical of ISF vectors in the system corresponding to three different levels of $c_{k\text{-}\ell}$ sparsity, with $c_{272\text{-}268}$ most sparse and $c_{112\text{-}148}$ least. Using a model of the 300-bus test system, benchmark values for $\Psi_{272\text{-}268}$, $\Psi_{30\text{-}73}$, and $\Psi_{112\text{-}148}$ are computed based on the definition of the ISF in (10), to which we compare estimates obtained via greedy pursuit (OMP), convex relaxation (log-barrier), and LSE algorithms. The original ISF vectors, ordered by the somewhat arbitrary network diagram designation (see, e.g., [29]), are neither sparse nor particularly smooth. As in Example 1, the PMU measurements have slight fluctuations in active-power injection at each bus via (17), from which one obtains the matrix ΔP, the regressor matrix used in ISF estimation for any line of interest. Next, the elements of each ISF vector are reordered by the electrical distance of each node to the line of interest and subsequently the columns of ΔP to obtain ΔP_s. Furthermore, the power flowing through each of lines $L_{272\text{-}268}$, $L_{30\text{-}73}$, and $L_{112\text{-}148}$ are computed for each set of bus injection data. From these computations, the observation vectors $\Delta P_{272\text{-}268}$, $\Delta P_{30\text{-}73}$, and $\Delta P_{112\text{-}148}$ are obtained, which are then substituted into (25) to solve via the OMP and log-barrier algorithms.

To assess the effectiveness of the proposed sparse vector recovery methods, several values of $m < n$ are chosen, corresponding to the number of synchronized data sets available. For each test case, one selects m rows from ΔP, reorders columns of ΔP by electrical distance away from line $L_{k\text{-}\ell}$, and finally multiplies by the inverse difference transformation matrix to obtain the measurement matrix Φ, as in (25). Combined with active line flows computed via MATPOWER, the sparse vector recovery problem in (25) is solved using the two algorithms described in Sect. 3.2: OMP in the class of greedy pursuit algorithms (with $\epsilon = 10^{-5}$) and log-barrier in the class of convex optimization algorithms (with $\eta = 10^{-5}$). The resulting vectors are sparse representations, denoted by $\widehat{c}_{k\text{-}\ell}$, of the ISF vector estimates, denoted by $\widehat{\Psi}_{k\text{-}\ell,s}$, which are obtained by applying the inverse difference transformation to $\widehat{c}_{k\text{-}\ell}$, as described in (24). For comparison, the estimates $\widehat{\Psi}_{k\text{-}\ell}$ are compared to the LSE-based method described in [7]. Finally, the accuracy of these three methods is evaluated against the benchmark ISF vectors obtained via direct model-based computation using the definition in (10). The results are described below and summarized in Table 3.

In the case of line $L_{272\text{-}268}$, one computes estimates via the OMP and log-barrier algorithm with $m = 110, 120, 130, 140$, and LSE with $m = 305, 350, 400, 600$. The log-barrier algorithm results in higher accuracy with only 130 sets of synchronized measurements as compared to the LSE with 600 sets. On the other hand, in the case of line $L_{30\text{-}73}$, the estimate obtained via log-barrier with 230 sets of measurements is about as accurate as that obtained using LSE with 400 sets. Regrettably, in the case of line $L_{112\text{-}148}$, estimates obtained via the proposed sparsity-exploiting methods

Table 3 Comparison between $\widehat{\Psi}_{k\text{-}\ell}$ and $\Psi_{k\text{-}\ell}$ for several lines in the IEEE 300-bus system

Line	$\|\|\widehat{\Psi}_{k\text{-}\ell} - \Psi_{k\text{-}\ell}\|\|_2$			
$L_{272\text{-}268}$	$m = 110$	$m = 120$	$m = 130$	$m = 140$
via OMP	0.0676	0.0693	0.0551	0.0777
via log-barrier	0.0320	0.0341	0.0271	0.0279
via LSE	$m = 305$	$m = 350$	$m = 400$	$m = 600$
	0.5891	0.0962	0.0678	0.0339
$L_{30\text{-}73}$	$m = 190$	$m = 210$	$m = 230$	$m = 250$
via OMP	0.0640	0.0649	0.0517	0.0494
via log-barrier	0.0320	0.0323	0.0268	0.0288
via LSE	$m = 305$	$m = 350$	$m = 400$	$m = 600$
	0.2719	0.0372	0.0236	0.0162
$L_{112\text{-}148}$	$m = 230$	$m = 250$	$m = 270$	$m = 290$
via OMP	0.9216	0.8255	0.7809	0.0964
via log-barrier	0.0849	0.0716	0.0377	0.0474
via LSE	$m = 305$	$m = 350$	$m = 400$	$m = 600$
	0.1414	0.0289	0.0168	0.0116

with as many as 290 sets of measurements are unable to surpass those obtained via the LSE method with as few as 350 sets. This decline in performance can be attributed to the sparsity level of the post-transformation ISF vector, $c_{k\text{-}\ell}$. In this case study, $c_{272\text{-}268}$ is the most sparse, followed by $c_{30\text{-}73}$, and then $c_{112\text{-}148}$. For lines for which the post-transformation ISF vector is not sparse, it may be prudent to search for an alternate representation that is sparse.

Also, in general, the estimates obtained via log-barrier are more accurate than those via OMP using the same observation matrix, which stems from the interior point convex optimization's insensitivity to the sparsity of the solution. Hence, OMP is able to produce good estimates even for non-sparse solutions, given enough measurement sets. As shown in the next case study involving the 2383-bus Polish power system, while the log-barrier method may be more robust, OMP is more superior if the solution is sparse.

4.2 Polish 2383-Bus System

For the Polish 2383-bus large-scale test case with 2896 lines [32], the effectiveness is evaluated of the electrical distance-based method proposed in Sect. 3.2 to sparsify ISF vectors as well as the OMP and log-barrier algorithms to estimate the resulting sparse vectors via the solution of (25).

4.2.1 Sparsify via Electrical Distance-Based Method

The benchmark ISFs for all lines in the Polish 2383-bus test system are computed by linearizing the nonlinear AC power flow equations. A measure is obtained for the sparsity of the pre-transformation ISF vector $\Psi_{k\text{-}\ell}$ by counting the number of nonzero elements in each normalized ISF vector with[4]

$$\kappa_{\Psi_{k\text{-}\ell}} = \#\left\{ i \in [1, n] : \frac{|\Psi^i_{k\text{-}\ell}|}{||\Psi_{k\text{-}\ell}||_\infty} > 0.005 \right\}. \tag{26}$$

Similarly, a comparable sparsity measure is obtained for the post-transformation vector $c_{k\text{-}\ell}$ with

$$\kappa_{c_{k\text{-}\ell}} = \#\left\{ i \in [1, n] : \frac{|c^i_{k\text{-}\ell}|}{||c_{k\text{-}\ell}||_\infty} > 0.005 \right\}. \tag{27}$$

The sparsity measures in (26) and (27) for all lines are visualized as histograms in Figs. 4 and 5, respectively. By comparing Figs. 4 and 5, we note that there is an increase in the number of vectors with fewer nonzero entries in the post-transformation $c_{k\text{-}\ell}$'s in Fig. 5 as compared to the pre-transformation $\Psi_{k\text{-}\ell}$'s in Fig. 4. In fact, $\kappa_{c_{k\text{-}\ell}} < 600$ for 92% of the lines, whereas $\kappa_{\Psi_{k\text{-}\ell}} < 600$ for 54%. Also, it is noted here that the pre-transformation ISF vectors of many lines are already highly sparse, as shown by the leftmost bar in Fig. 4. The high degree of sparsity is in agreement with the intuition that, in a large-scale system, many line flows are significantly affected by only a small number of nodal injections. In these cases, the transformation proposed in Sect. 3.2 does not affect the sparsity of the corresponding post-transformation ISF vector.

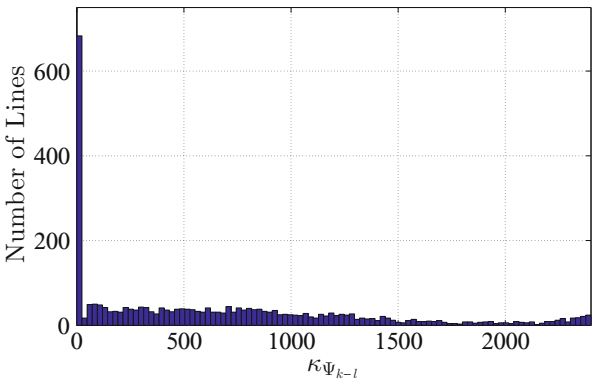

Fig. 4 Polish 2383-bus system: Sparsity of pre-transformation $\Psi_{k\text{-}\ell}$ vectors

[4] $\#\mathcal{A}$ denotes the cardinality of set $\mathcal{A}$.

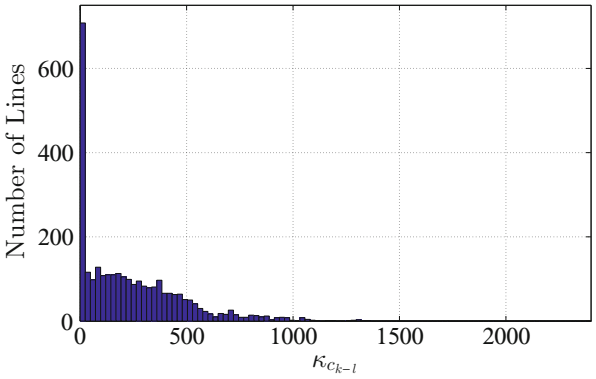

Fig. 5 Polish 2383-bus system: Sparsity of post-transformation $c_{k\text{-}\ell}$ vectors

Table 4 Comparison between $\widehat{\Psi}_{k\text{-}\ell}$ and $\Psi_{k\text{-}\ell}$ for the Polish 2383-bus system case study

Line	$\|\|\widehat{\Psi}_{k\text{-}\ell} - \Psi_{k\text{-}\ell}\|\|_2$			
$L_{53\text{-}52}$	$m = 500$	$m = 600$	$m = 700$	$m = 800$
via OMP	0.0490	0.0480	0.0413	0.0402
via log-barrier	0.0562	0.0516	0.0459	0.0391

Table 5 Timing comparison for Polish 2383-bus system case study

Line	Execution Time [s]			
$L_{53\text{-}52}$	$m = 500$	$m = 600$	$m = 700$	$m = 800$
via OMP	0.2798	0.4502	0.5263	0.7828
via log-barrier	15.5302	13.7511	15.8118	16.1992

4.2.2 Sparse ISF Vector Recovery

To illustrate the effectiveness of the proposed DEPS algorithms, the ISFs of line $L_{53\text{-}52}$ are considered with respect to each of the 2383 buses in the system. Due to the size of the 2838 test system and the resulting exorbitant simulation time, it is not practical to compute $\widehat{\Psi}_{k\text{-}\ell}$ estimates directly using the LSE-based method. As in the 300-bus case study, a sparse representation of the ISF vector is employed and estimates via OMP (for $\epsilon = 0.01$) and log-barrier method (for $\eta = 10^{-5}$) are computed. Then, these results are compared to benchmark ISF obtained using the model-based approach; the results are shown in Table 4. Here, unlike in the 300-bus case study, the solution is highly sparse and so the OMP algorithm results in more accurate ISF estimates than the log-barrier one from the same synchronized measurement sets (except for the case $m = 800$). Also, as shown in Table 5, the OMP algorithm incurs much lower computation time than the log-barrier one.

5 Concluding Remarks and Future Vision

This chapter outlined the DEPS method to estimate distribution factors through LSE estimation, which does not rely on the system power flow model, using online PMU measurements collected in real time. The LSE method is shown to accurately estimate ISFs. The chapter further presented a modified approach to estimate ISFs by exploiting a sparse representation of them to improve estimation performance. The application of this method was illustrated in the case of the IEEE 14-bus, the IEEE 300-bus, and the Polish 2383-bus large-scale test systems. The estimated ISFs can then be incorporated into existing real-time contingency analysis that rely on sensitivities computed from an offline system model. The offline model is prone to mismatch with the actual system in real-time operations, which may lead to erroneous power system security analysis results. The DEPS methods presented in this chapter avoid such errors by using online measurements to directly estimate sensitivities of interest.

Our generation is witness to radical transformations within the power system infrastructure, which includes the integration of many emerging technologies, such as renewable-based electricity generation and advanced sensors. Along with challenges that arise due to these changes, there are vast opportunities to improve upon existing power system analysis tools. The DEPS methods discussed in this chapter represent only a fraction of the effort to develop DDDAS-based monitoring and operations tools in order to satisfy the needs of power system security assessment and protection tasks in the coming decades. With regard to this, the potential held by widespread deployment of advance sensors throughout the grid is monumental, and these sensors ought to be fully exploited to perform inference and estimation, as well as aid in analysis and decision-making. Moving forward, a symbiotic relationship, as sketched in Fig. 1, between the traditional model-based and contemporary DDDAS-based paradigms will enable efficient and robust online security assessment. This chapter offered a few building blocks toward the grand vision, which still requires much more work to be fully realized.

References

1. FERC and NERC, “Arizona-Southern California outages on September 8, 2011: Causes and recommendations.” [online], Apr. 2012. Available at http://www.ferc.gov/legal/staff-reports/04-27-2012-ferc-nerc-report.pdf.
2. U.S.-Canada Power System Outage Task Force, “Final report on the August 14th blackout in the united states and Canada: causes and recommendations.” [online], Apr. 2004. Available at https://reports.energy.gov/BlackoutFinal-Web.pdf.
3. A. Wood and B. Wollenberg, *Power Generation, Operation and Control*. New York: Wiley, 1996.
4. E. Blasch, S. Ravela, and A. Aved, eds., *Handbook of Dynamic Data Driven Applications Systems*. Springer, 2018.
5. Z. Dong and P. Zhang, *Emerging Techniques in Power System Analysis*. Springer-Verlag, 2010.

6. US DOE & FERC, "Steps to establish a real-time transmission monitoring system for transmission owners and operators within the eastern and western interconnections." [online], Feb. 2006. Available at http://energy.gov.
7. Y. C. Chen, A. D. Domínguez-García, and P. W. Sauer, "Online computation of power system linear sensitivity distribution factors," in *Proc. of the IREP Bulk Power System Dynamics and Control Symposium*, Aug. 2013.
8. Y. C. Chen, A. D. Domínguez-García, and P. W. Sauer, "Measurement-based estimation of linear sensitivity distribution factors and applications," *IEEE Transactions on Power Systems*, vol. 29, pp. 1372–1382, May 2014.
9. Y. C. Chen, A. D. Domínguez-García, and P. W. Sauer, "Online estimation of power system distribution factors—a sparse representation approach," in *Proc. of the North American Power Symposium*, Sept. 2013.
10. Y. C. Chen, A. D. Domínguez-García, and P. W. Sauer, "A sparse representation approach to online estimation of power system distribution factors," *IEEE Transactions on Power Systems*, vol. 30, pp. 1727–1738, Jul 2015.
11. P. Sauer, "On the formulation of power distribution factors for linear load flow methods," *IEEE Transactions on Power App. Syst.*, vol. PAS-100, pp. 764–779, Feb. 1981.
12. B. Stott, J. Jardim, and O. Alsac, "DC power flow revisited," *IEEE Transactions on Power Systems*, vol. 24, no. 3, pp. 1290–1300, 2009.
13. T. Güler, G. Gross, and M. Liu, "Generalized line outage distribution factors," *IEEE Transactions on Power Systems*, vol. 22, no. 2, pp. 879–881, 2007.
14. J. Guo, Y. Fu, Z. Li, and M. Shahidehpour, "Direct calculation of line outage distribution factors," *IEEE Transactions on Power Systems*, vol. 24, no. 3, pp. 1633–1634, 2009.
15. Y. C. Chen, J. Wang, A. D. Domínguez-García, and P. W. Sauer, "Measurement-based estimation of the power flow Jacobian matrix," *IEEE Transactions on Smart Grid*, vol. 7, no. 5, pp. 2507–2515, 2016.
16. Y. C. Chen, T. Banerjee, A. D. Domínguez-García, and V. V. Veeravalli, "Quickest line outage detection and identification," *IEEE Transactions on Power Systems*, vol. 31, no. 1, pp. 749–758, 2016.
17. A. Al-Digs, S. V. Dhople, and Y. C. Chen, "Dynamic distribution factors," *IEEE Transactions on Power Systems*, vol. 34, no. 6, pp. 4974–4983, 2019.
18. A. Al-Digs, S. V. Dhople, and Y. C. Chen, "Measurement-based sparsity-promoting optimal control of line flows," *IEEE Transactions on Power Systems*, vol. 33, no. 5, pp. 5628–5638, 2018.
19. G. Rovatsos, X. Jiang, A. D. Domínguez-García, and V. V. Veeravalli, "Statistical power system line outage detection under transient dynamics," *IEEE Transactions on Signal Processing*, vol. 65, no. 11, pp. 2787–2797, 2017.
20. S. Nowak, Y. C. Chen, and L. Wang, "Measurement-based optimal der dispatch with a recursively estimated sensitivity model," *IEEE Transactions on Power Systems*, vol. 35, no. 6, pp. 4792–4802, 2020.
21. S. Haykin, *Adaptive Filter Theory*. Prentice Hall, 1996.
22. F. Schweppe, *Uncertain Dynamic Systems*. Englewood Cliffs, NJ: Prentice-Hall Inc., 1973.
23. Y. C. Eldar and G. Kutyniok, *Compressed sensing: theory and applications*. Cambridge University Press, 2012.
24. H. Zhu and G. B. Giannakis, "Sparse overcomplete representations for efficient identification of power line outages," *IEEE Transactions on Power Systems*, vol. 27, no. 4, pp. 2215–2224, 2012.
25. D. L. Donoho, "Compressed sensing," *IEEE Transactions on Information Theory*, vol. 52, no. 4, pp. 1289–1306, 2006.
26. E. J. Candès, J. Romberg, and T. Tao, "Robust uncertainty principles: Exact signal reconstruction from highly incomplete frequency information," *IEEE Transactions on Information Theory*, vol. 52, no. 2, pp. 489–509, 2006.
27. A. Conejo, J. Contreras, D. Lima, and A. Padilha-Feltrin, "Zbus transmission network cost allocation," *IEEE Transactions on Power Systems*, vol. 22, pp. 342–349, Feb. 2007.

28. J. Tropp and S. Wright, "Computational methods for sparse solution of linear inverse problems," *Proceedings of the IEEE*, vol. 98, pp. 948–958, June 2010.
29. University of Washington, "Power system test case archive." [online], Oct. 2012. Available at http://www.ee.washington.edu/research/pstca/.
30. R. D. Zimmerman, C. E. Murillo-SǴnchez, and R. J. Thomas, "MATPOWER: Steady-state operations, planning and analysis tools for power systems research and education," *IEEE Transactions on Power Systems*, vol. 26, pp. 12–19, Feb. 2011.
31. Electric Grid Test Case Repository, "IEEE 300-bus system." [online], 2020. Available at https://electricgrids.engr.tamu.edu/electric-grid-test-cases/ieee-300-bus-system/.
32. MATPOWER, "CASE2383WP power flow data for polish system." [online], 2020. Available at https://matpower.org/docs/ref/matpower5.0/case2383wp.html.